

Supporting Information

Electron-Donating Strategy to Guide the Construction of MOF Photocatalysts toward Co-Catalyst-Free High-Efficient Photocatalytic Protons Reduction

Dapeng Dong, Chaoxiong Yan, Jindou Huang, Na Lu, Pengyan Wu,* Jian Wang, and Zhenyi Zhang**

Dr. D. Dong, C. Yan, Dr. J. Huang, Dr. N. Lu, Prof. Z. Zhang
Key Laboratory of New Energy and Rare Earth Resource Utilization of State Ethnic Affairs Commission
Key Laboratory of Photosensitive Materials and Devices of Liaoning Province
School of Physics and Materials Engineering
Dalian Nationalities University
18 Liaohe West Road, Dalian 116600, P. R. China
E-mail: jindouhuang@dlnu.edu.cn; zhangzy@dlnu.edu.cn

Dr. P. Wu, Dr. J. Wang
School of Chemistry and Materials Science
Jiangsu Normal University
Xuzhou, 221116, P. R. China
E-mail: wpyan@jsnu.edu.cn

Prof. Z. Zhang
School of Materials Science and Engineering
Zhengzhou University
Zhengzhou, 450001, P. R. China

Experimental Section

Materials and Characterizations

All the chemicals were purchased from commercial sources and used without any further purification. Elemental analyses of C, H, N and S were carried out with a PE-2400 elemental analyzer. Contents of Cd were analysed through the inductively coupled plasma (ICP) by using a NexION 1000 ICP Mass Spectrometer. IR spectra were recorded on a Thermo Scientific Nicolet iS10 FT-IR Spectrometer with KBr pellets in the range 4000–400 cm^{-1} . Powder XRD patterns were obtained using a Bruker D8 ADVANCE XRD diffractometer with $\text{CuK}\alpha$ radiation ($\lambda = 1.54056 \text{ \AA}$). The thermogravimetric (TG) analysis were performed using a Perkin–Elmer Pyris Diamond TG-DTA thermal analyses system in a nitrogen atmosphere on polycrystalline samples with a heating rate of 10 K min^{-1} from 50 to 800 $^{\circ}\text{C}$. The UV–vis diffuse reflectance (DR) spectra of the samples were recorded on a Lambda 750 UV–Vis–NIR spectrophotometer (Perkin-Elmer, USA). Decay curves of the as-fabricated products were obtained on a FLS920 fluorescence lifetime spectrophotometer (Edinburgh Instruments, UK). The electron paramagnetic resonance (EPR) spectra were performed on the MOF samples by using a Bruker EPR A200 spectrometer through trapping with 5, 5-Dimethyl-1-pyrroline N-oxide (DMPO). The sample in the DMPO aqueous solution were oscillated to make the photocatalyst blend evenly, added into an EPR quartz tube, and irradiated with a 300W Hg lamp. The settings for the EPR spectrometer were as follows: center field = 3320 G, microwave frequency = 9.30 GHz, sweep width = 200 G, modulation frequency = 100 kHz, and power = 6.36 mW.

Photocatalytic H₂ Evolution

For photocatalytic H₂ evolution tests, each sample was put into a 10 mL flask with a volume of 5 mL in water. Typically, the sample contained 1 mg DLNU-M-CdS(H₂TD) and 15% (v/v) TEOA (or 1 mg DLNU-M-CdS(H₂TD)(H₂O) and 10% (v/v) TEOA) as the sacrificial electron donor. The flask was sealed with a septum and

protected from light, then degassed by bubbling nitrogen for 25 min under atmospheric pressure at room temperature. After that, the samples were irradiated by a 300 W Xenon lamp, the reaction temperature was 293 K by using a water filter to absorb heat. The generated photoproduct of H₂ was characterized by GC 7890T instrument analysis using a 5 Å molecular sieve column (0.6 m × 3 mm), thermal conductivity detector, and nitrogen used as carrier gas. The amount of hydrogen generated was determined by the external standard method.

Computational Methods

The DOS calculations of DLNU-M-CdS(H₂TD) and DLNU-M-CdS(H₂TD)(H₂O) MOF were implemented in the Vienna ab initio Simulation Package (VASP) code. The geometry optimizations are performed using the frozen-core projector-augmented-wave (PAW) method and the generalized gradient approximation (GGA) for exchange correlation. The cutoff energy for the plane-wave basis set is 500 eV and the force on each atom is converged to 0.01 eV/Å for all structural relaxations. A set of 4×4×4 Monkhorst-Pack special k-points has been used for structural relaxations to search for the most stable configurations. The optimized lattice parameters for DLNU-M-CdS(H₂TD) MOF are a = 11.647 Å, b = 13.703, and c = 8.017 Å, and the ones for DLNU-M-CdS(H₂TD)(H₂O) MOF are a = 6.869 Å, b = 14.589, and c = 7.098 Å, which are in agreement with experimental values. Density of states (DOS) calculations of DLNU-M-CdS(H₂TD) and DLNU-M-CdS(H₂TD)(H₂O) MOF systems were investigated by employing the range-separated hybrid Heyd-Scuseria-Ernzerh (HSE06) of exchange and correlation functional. The HSE06 functional is a screened exchange functional, and we set the range separation parameter (μ) to 0.2 Å⁻¹. At short range a mixing of 25% of exact Hartree-Fock (HF) and 75% of Perdew-Burke-Ernzerhof (PBE) exchange is used, while at long range the standard PBE exchange is maintained. The predicted band gaps of DLNU-M-CdS(H₂TD) and DLNU-M-CdS(H₂TD)(H₂O) MOF are 3.32eV and 3.89eV, respectively, which are consistent with the experimental values.

Photoelectrochemical measurements

Transient photocurrent, incident photon-to-electron conversion efficiency (IPCE) tests and Mott–Schottky (MS) plots were obtained using a CHI 660D electrochemical workstation (Chenhua Instrument, Shanghai, China) in a conventional three-electrode configuration using a Pt foil as the counter electrode and Ag/AgCl (saturated with KCl) as the reference electrode. To prepare the working electrodes, 5 mg of the photocatalyst was mixed with 0.1 mL ethanol to form a paste, then the above paste was placed over an In-doped SnO₂ (ITO) glass (effective area of 1 cm × 1 cm), and a drop of Nafion ethanol solution (1 wt %) was placed on the surface. A 0.1 M Na₂SO₄ aqueous solution was used as the electrolyte, and the solution was degassed by purging N₂ gas for 10 min before irradiation. Then, a 300-W Xe lamp (NBET, HSX-F300) equipped with a monochromator (NBET) was used to irradiate the as-prepared working electrode.

The IPCE measurements were performed under the same conditions, in which the monochromatic light irradiation was provided by the same Xe lamp.

The incident photon-to-current-conversion efficiency (IPCE) measurement with different excitation wavelengths give further evidence at the above viewpoint. Its standard equation can be expressed as

$$IPCE = \frac{1240I}{\lambda J_{light}} \times 100\% \quad (1)$$

Where λ denotes the incident light wavelength; J_{light} is the incident light power density, and I is the photocurrent density.

The Mott–Schottky (M–S) plots were also recorded using the CHI660E three-electrode system at an AC frequency of 1 kHz, with the amplitude as 20 mV vs. Ag/AgCl, the electrolyte was a neutral aqueous solution containing 0.5 M Na₂SO₄. All these experiments were conducted under dark conditions.

The electrochemical flat-band potentials (E_{fb}) of the as-fabricated samples were measured using Mott–Schottky plots based on the following equation

$$\frac{1}{C^2} = \frac{2}{\epsilon\epsilon_0 N_D} \left(E - E_{fb} - \frac{k_B T}{q} \right) \quad (2)$$

Where C denotes the space charge capacitance; N_D , ϵ , and ϵ_0 represent the donor density, dielectric constant of the semiconductor film electrode, and permittivity in vacuum, respectively; E is the applied potential; and q , k_B , and T are the electronic charge, Boltzmann's constant, and absolute temperature, respectively.

Apparent quantum efficiency measurement

The apparent quantum efficiency (AQE) was measured at 365 nm by using a band pass filter (half width: 15 nm) under the identical reaction condition for H_2 production. The number of incident photons from the 300-W xenon lamp (CEL-HXF300, CEAULIGHT Co. Ltd.) is measured with a power meter (70260, Newport Corp.). The AQE value can be calculated by using the following equation:

$$AQE = \frac{2 \times \text{number of evolved hydrogen molecules}}{\text{number of incident photons}} \times 100\% \quad (3)$$

The apparent quantum efficiency is $\sim 1.38\%$ for the DLNU-M-CdS(H_2TD).

Synthesis of CdS-based MOFs

(1) **Synthesis of DLNU-M-CdS(H_2TD)**: Hydrothermal treatment of CdI_2 (0.073 g, 0.2 mmol), H_2TD (0.015 g, 0.1 mmol) and water (10 mL) for 3 d at 140 °C yielded crystalline yellow block. The yield of **1** was about 55 % based on Cd. Elemental analysis for compound **1**: Calc (found) for $C_2CdN_2S_3$: %C 9.22 (9.26), %N 10.75 (10.78), %S 36.91 (36.86). IR (KBr cm^{-1}): 1374(w), 1355(s), 1344(s), 1087(m), 1067(s), 1045(w), 1039(w), 770(w), 666(w).

(2) **Synthesis of DLNU-M-CdS(H_2TD)(H_2O)**: Hydrothermal treatment of $CdCl_2 \cdot 5/2H_2O$ (0.023 g, 0.1 mmol), H_2TD (0.015 g, 0.1 mmol), DMF (2.0 mL), $NH_3 \cdot H_2O$ (1.0 mL) and water (8.0 mL) for 3 d at 140 °C yielded crystalline light yellow block. The yield of **2** was about 49% based on Cd. Elemental analysis for compound **2**: Calc (found) for $C_2H_2CdN_2OS_3$: %C 8.62 (8.68), %N 10.05 (10.10), %H 0.72 (0.74), %S 34.52 (34.47). IR (KBr cm^{-1}): 3432(br), 1384(m), 1355(s), 1344(s), 1087(m), 1067(s), 1045(w), 1039(w), 770(w), 664(w).

Crystallographic studies

Data collections for DLNU-M-CdS(H₂TD) (**1**) and DLNU-M-CdS(H₂TD)(H₂O) (**2**) were performed on a Bruker AXS Smart APEX II CCD X–diffractometer equipped with graphite monochromated Mo–K α radiation ($\lambda = 0.71073\text{\AA}$) at 293 ± 2 K. An empirical absorption correction was applied using the SADABS program. The structures were solved by direct methods and refined by full matrix least–squares on F^2 by using the program SHELXL–2014. All non-hydrogen atoms were refined with anisotropic thermal parameters. Hydrogen atoms of organic ligands were generated geometrically with fixed isotropic thermal parameters, and included in the structure factor calculations. Details of crystallographic data and structural refinements of DLNU-M-CdS(H₂TD) (**1**) and DLNU-M-CdS(H₂TD)(H₂O) (**2**) were summarized in Table S1. The CCDC 1912087 and 1912088 containing the supplementary crystallographic data were provided for this paper.

Calculations of Lifetimes for the Photoinduced Charge-Carriers through the Time-Resolved photoluminescence (TRPL) Decay Curves

The TRPL decay curves of these two samples can be mathematically described as the following biexponential function:^[1]

$$I(t) = A_1 \cdot \exp(-t/\tau_1) + A_2 \cdot \exp(-t/\tau_2) \quad \text{Equation (S1)}$$

Where τ_1 and τ_2 are the fluorescent lifetime, and A_1 , and A_2 are the corresponding amplitudes.

The average fluorescent lifetimes of these two samples can be obtained according to the following equation:^[1]

$$\tau_A = \frac{A_1 \cdot \tau_1^2 + A_2 \cdot \tau_2^2}{A_1 \cdot \tau_1 + A_2 \cdot \tau_2} \quad \text{Equation (S2)}$$

The dynamics process of photoinduced charge-carriers can be further deduced through the electron-transfer rate constants expressed as follow:^[2]

$$k_{et}(\text{MOF/Protons}(\text{in TEOA solution}) \rightarrow \text{MOF}(\text{in water}))$$

$$= \frac{1}{\langle \tau_A \rangle_{(\text{MOF/Protons})}} - \frac{1}{\langle \tau_A \rangle_{(\text{MOF})}}$$

Equation (S3)

Table S1 Crystallographic data for DLNU-M-CdS(H₂TD) (**1**) and DLNU-M-CdS(H₂TD)(H₂O) (**2**)

Compound	1	2
formula	C ₂ CdN ₂ S ₃	C ₂ CdN ₂ S ₃ ·H ₂ O
Fw	260.62	278.64
crystal system	Monoclinic	Monoclinic
Space group	<i>C2/c</i>	<i>P2₁/n</i>
<i>a</i> , Å	10.7038(10)	6.2918(4)
<i>b</i> , Å	13.7718(13)	15.1309(9)
<i>c</i> , Å	7.7097(7)	7.2767(4)
α , °	90	90
β , °	100.7600(10)	103.2113(6)
γ , °	90	90
<i>V</i> , Å ³	1116.51(18)	674.41(7)
<i>Z</i>	8	4
<i>D_c</i> , g/cm ³	3.101	2.744
μ (Mo <i>Kα</i>), mm ⁻¹	4.900	4.076
θ_{\min} , θ_{\max} , °	2.437, 27.507	2.692, 24.998
no. total reflns.	6325	4795
no. uniq. reflns (<i>R</i> _{int})	1282 (0.0205)	1184 (0.0192)
no. obs. [$I \geq 2\sigma(I)$]	1221	1155
no. params	73	83
<i>R</i> 1, <i>wR</i> 2 [$I \geq 2\sigma(I)$]	0.0151, 0.0385	0.0162, 0.0432
<i>R</i> 1, <i>wR</i> 2 (all data)	0.0163, 0.0393	0.0166, 0.0434
GOF	1.027	1.002

Table S2 Photocatalytic H₂-evolution rate of DLNU-M-CdS(H₂TD) with different hole-scavengers.

Sample	Methanol	Lactic Acid	Triethanolamine
DLNU-M-CdS(H ₂ TD)	0.83 mmol g ⁻¹ h ⁻¹	2.57 mmol g ⁻¹ h ⁻¹	26.1 mmol g ⁻¹ h ⁻¹

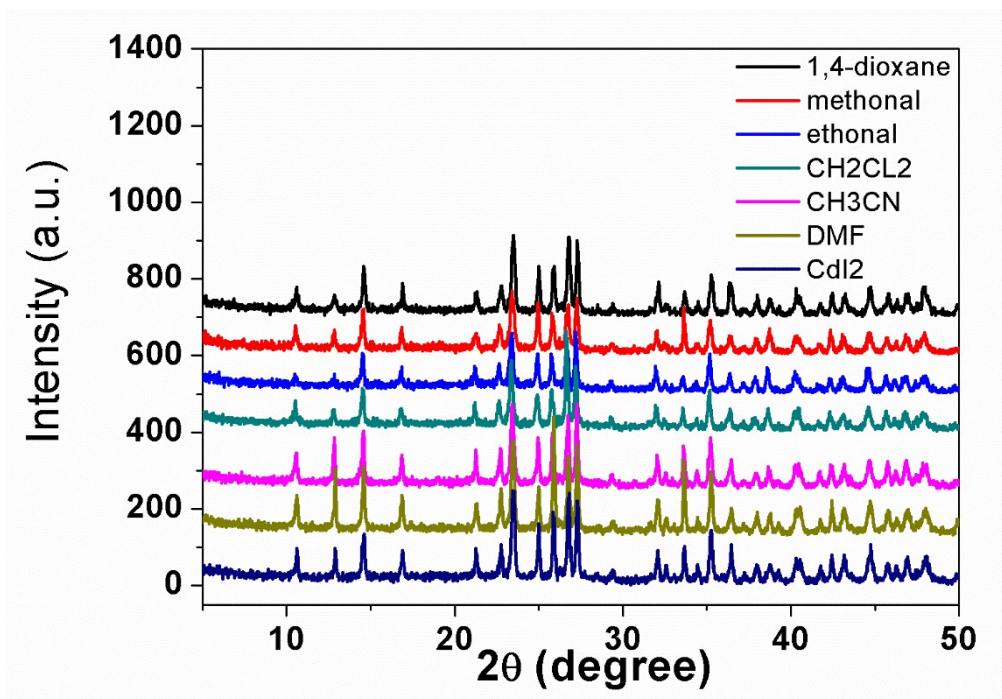


Fig. S1 XRD patterns of DLNU-M-CdS(H₂TD) after immersing in different solvents for 24 hours.

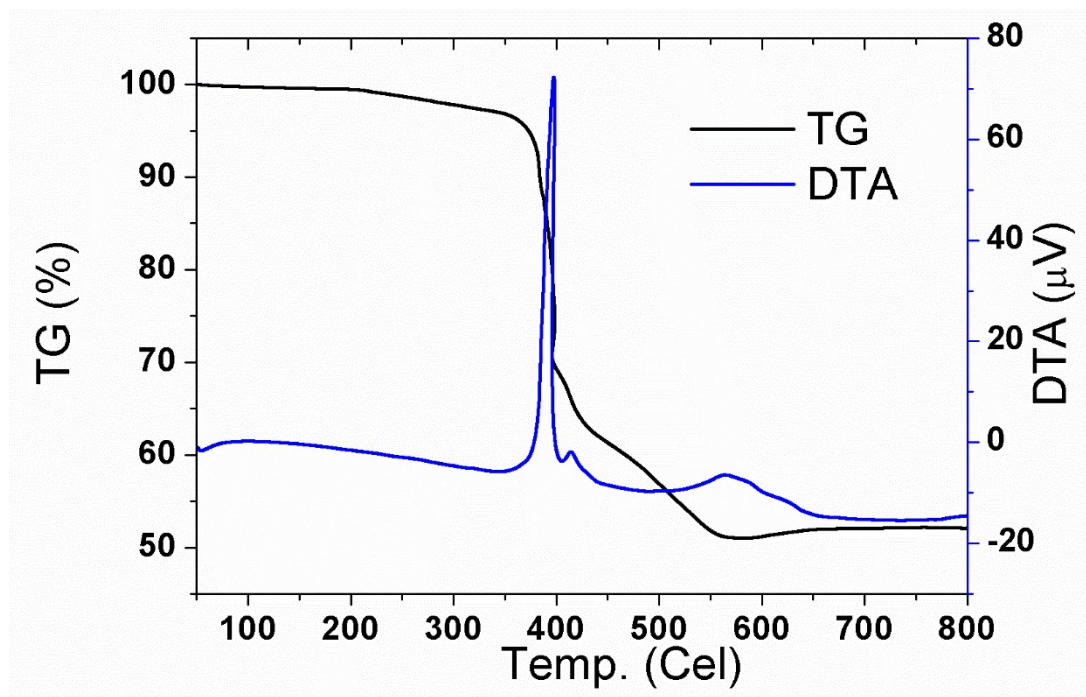


Fig. S2 The TG and DTA curves of DLNU-M-CdS(H₂TD).

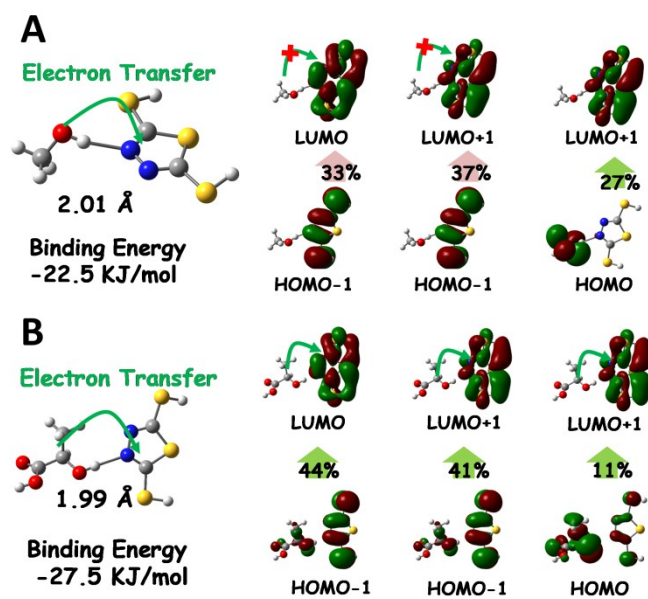


Fig. S3 The geometries of methanol-H₂TD (A) and lactic acid-H₂TD (B) complexes, and the shapes of frontier molecular orbitals related to their maximum absorption peaks.

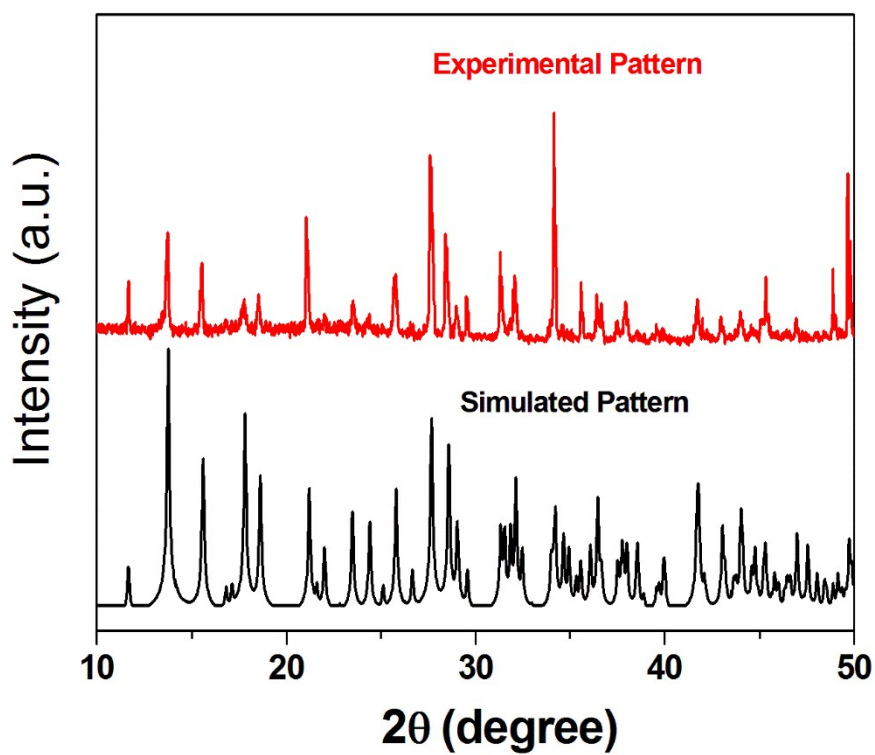


Fig. S4 The experimental and simulated XRD patterns of DLNU-M-CdS(H₂TD)(H₂O).

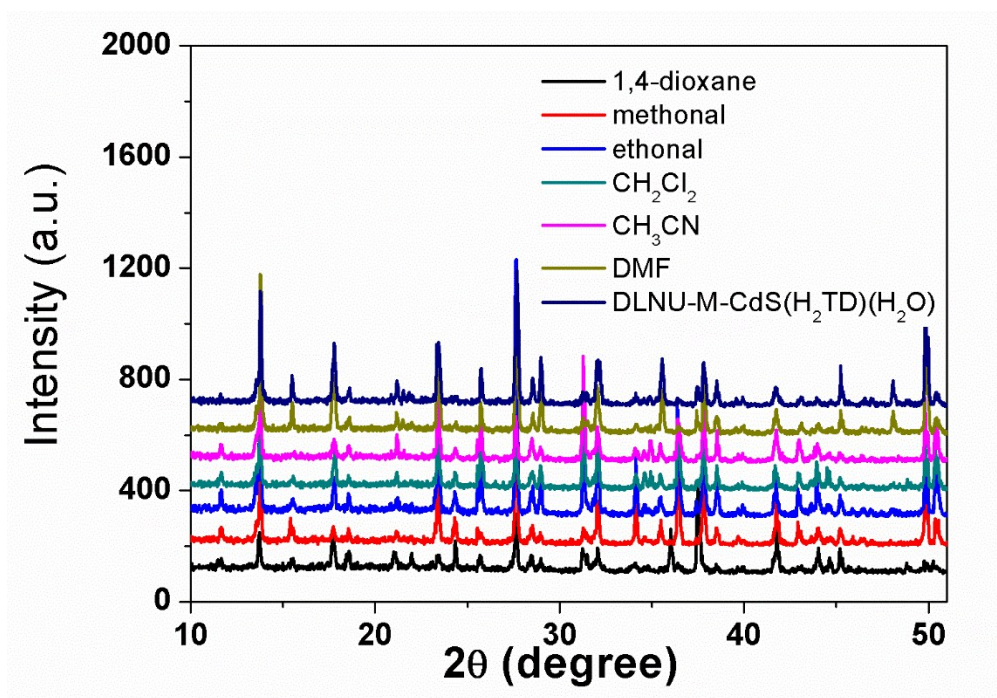


Fig. S5 XRD patterns of DLNU-M-CdS(H₂TD)(H₂O) after immersing in different solvents for 24 hours.

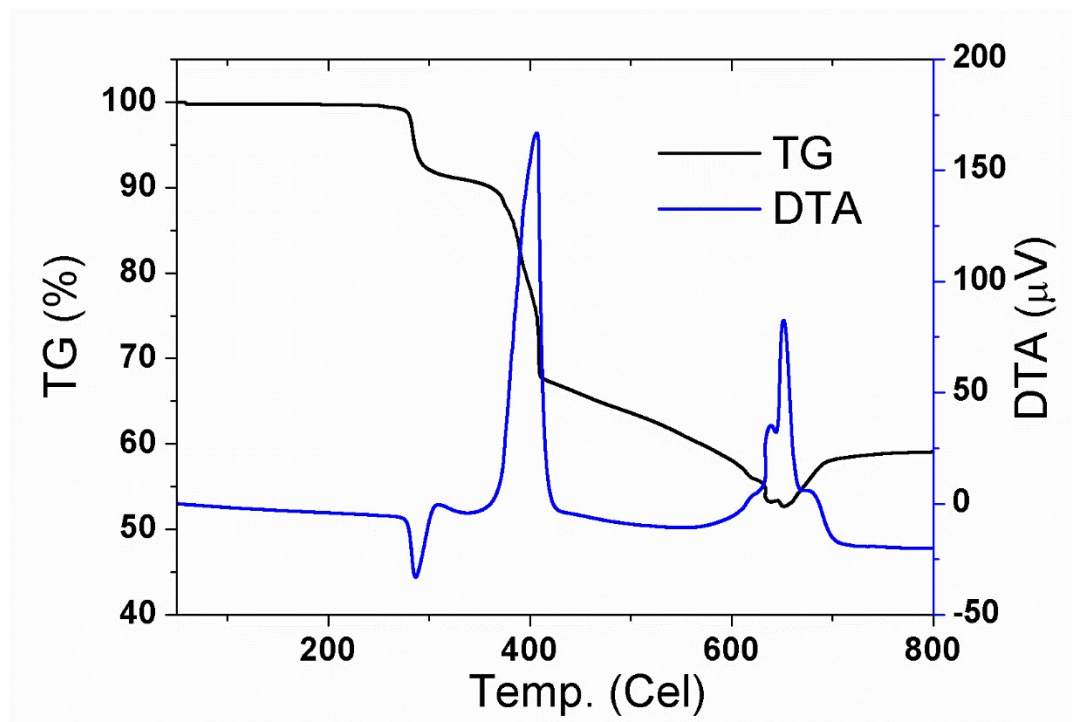


Fig. S6 The TG and DTA curves of DLNU-M-CdS(H₂TD)(H₂O).

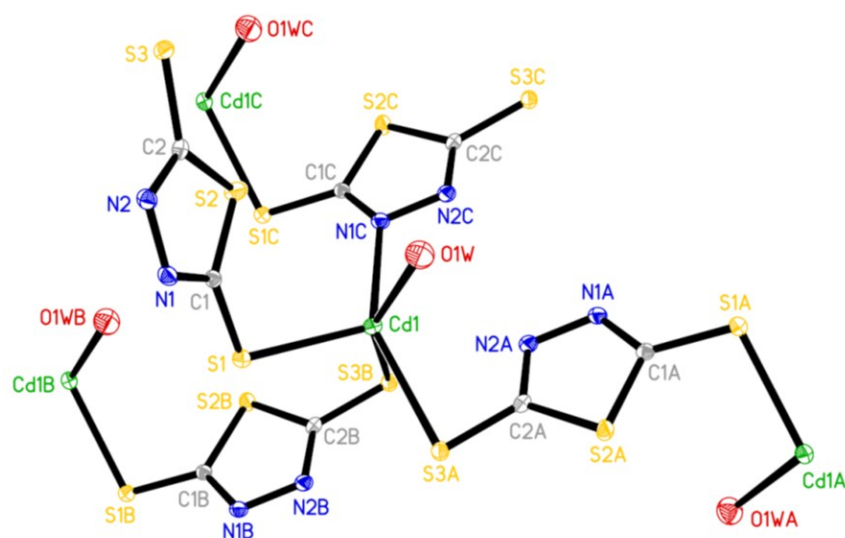


Fig. S7 Structure unit of DLNU-M-CdS(H₂TD)(H₂O) showing the atom labeling. Thermal ellipsoids are shown at the 30% probability level. All H atoms in water are omitted for clarity. Symmetry code for the generated atoms: (A) $x-1/2, -y+1/2, z+1/2$; (B) $-x-1/2, y+1/2, -z-1/2$; (C) $x+1/2, -y+1/2, z+1/2$.

Structure description of compound DLNU-M-CdS(H₂TD)(H₂O) (2).

Single-crystal X-ray diffraction analysis revealed that DLNU-M-CdS(H₂TD)(H₂O) crystallizes in the monoclinic space group $P2_1/n$. Each fundamentally structural unit contains four unique Cd(II) cations, four H₂TD ligands and four coordinated water molecules (Fig. S7). The Cd1 cation is five-coordinated environment, which is coordinated by three sulfur atoms (S1, S3A and S3B) from three separate TD²⁻ anions, one nitrogen atom (N1C) from one TD²⁻ anion and one coordinated water molecule to form the CdS₃NO polyhedral geometry. The TD ligand bridges three Cd cations through two terminal S atoms and one N atom to form 3D framework structure.

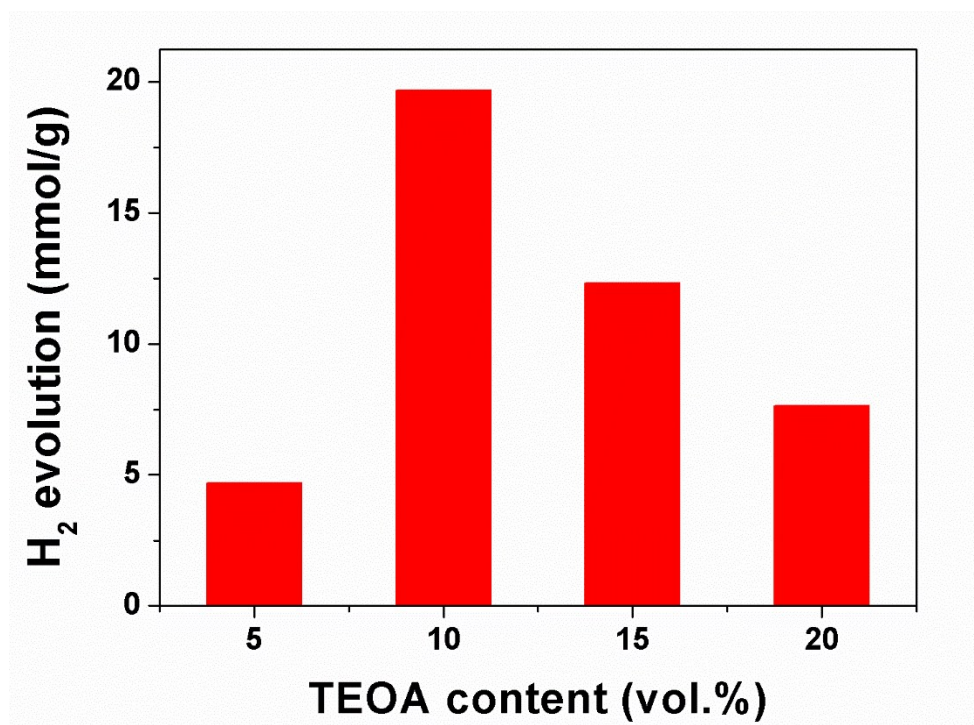


Fig. S8 H₂-evolution amount over DLNU-M-CdS(H₂TD)(H₂O) in aqueous solution containing different contents of TEOA under UV-visible-light irradiation for 3h.

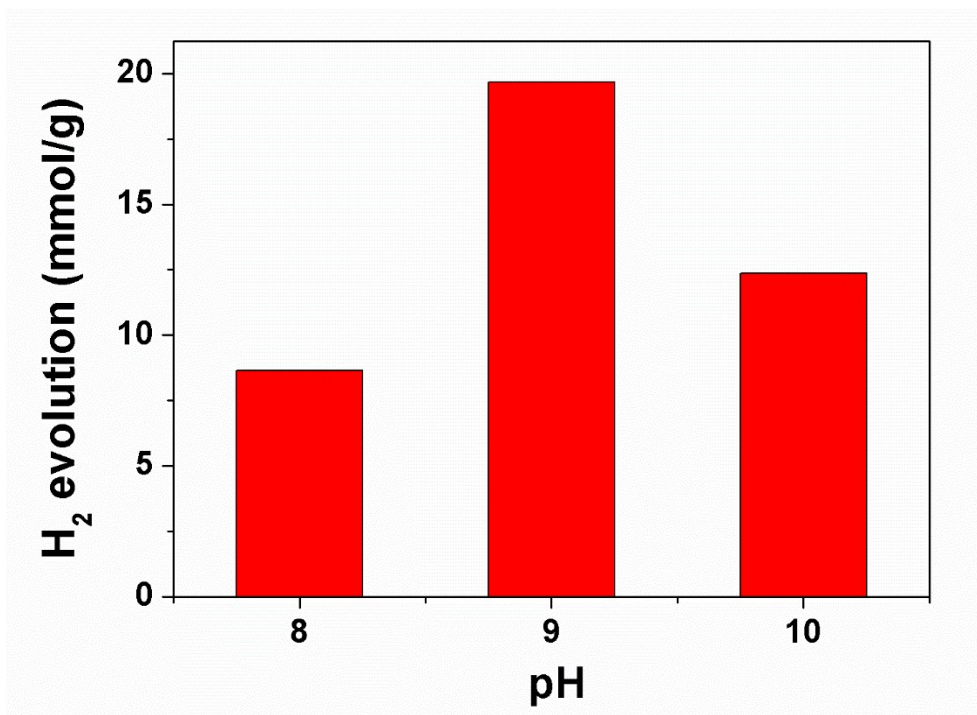


Fig. S9 H₂-evolution amount over DLNU-M-CdS(H₂TD)(H₂O) in 10 vol.% TEOA aqueous solution with different initial pH-values under UV-visible-light irradiation for 3h.

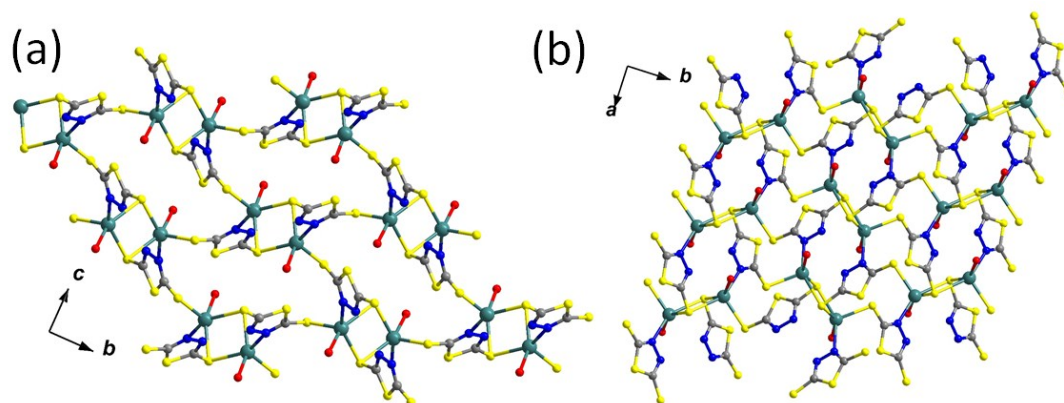


Fig. S10 (a) Ball and stick representation of DLNU-M-CdS(H₂TD)(H₂O) viewed along the c axis; (b) Ball and stick representation of DLNU-M-CdS(H₂TD)(H₂O) viewed along the b axis. All H atoms in water are omitted for clarity.

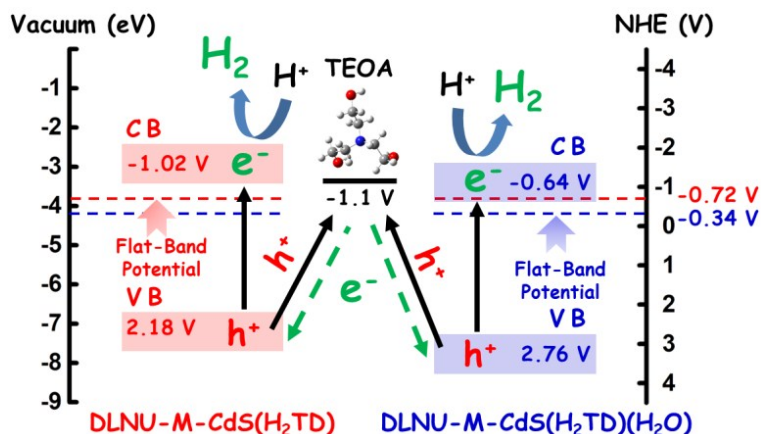


Fig. S11 Schematic diagram showing the energy band structures and electron transfer processes at the interface between the CdS-based MOFs and the TEOA.

The Mott-Schottky plots indicate that the flat-band potentials of DLNU-M-CdS(H₂TD) and DLNU-M-CdS(H₂TD)(H₂O) are about -0.72 and -0.34 V vs. NHE, respectively. Usually, the flat-band potential is ~0.3 V below the conduction band (CB) of the semiconductor.^[2] As a result, the CB potentials for the DLNU-M-CdS(H₂TD) and DLNU-M-CdS(H₂TD)(H₂O) can be calculated as -1.02 and -0.64 V vs. NHE, respectively. Furthermore, according to the UV-vis absorption spectra, the bandgaps of DLNU-M-CdS(H₂TD) and DLNU-M-CdS(H₂TD)(H₂O) are ~3.2 and ~3.4 eV, respectively. Thus, the valence band (VB) potentials are 2.18 and 2.76 eV for the DLNU-M-CdS(H₂TD) and DLNU-M-CdS(H₂TD)(H₂O), respectively (Fig. S11). Besides, the previous literature reported that TEOA has the oxidation potential (i.e., the weaker bound electron) with an electronic energy level at 3.4 eV vs. vacuum.^[3] Upon interband excitations of both two CdS-based MOFs, the photoinduced electrons on the VB of the MOFs can transfer to the CB, leaving the same amount of the holes on their VB. The photoinduced electrons on the CB of the MOFs are capable of initiating the photocatalytic protons reduction for H₂ evolution. Meanwhile, the photoinduced holes would quickly move to the hole-scavenger TEOA for oxidizing the TEOA due to the existence of deep hole-potential-wells between the

VB of CdS-based MOFs and the TEOA. In other word, the electrons in the TEOA would be easy to donate to the VB of the CdS-based MOFs for strongly hindering the photoinduced charge-carrier recombination of the MOFs.

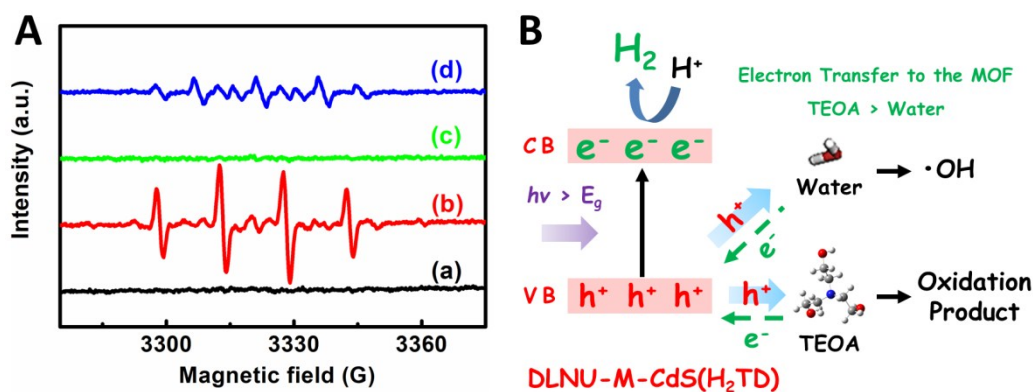


Fig. S12 (A) EPR spectra of the DLNU-M-CdS(H₂TD) MOF in the DMPO aqueous solution under different testing conditions: (a) in the dark; (b) UV-light irradiation for 2 min; in the DMPO-TEOA mixed aqueous (c) without light irradiation and (d) under UV-light irradiation for 2 min; (B) Schematic diagram showing the electron transfer process from water or TEOA to the MOF upon UV-light irradiation.

The electron paramagnetic resonance (EPR) spectra have been measured through mixing the DLNU-M-CdS(H₂TD) MOF in the 5,5-Dimethyl-1-pyrroline N-oxide (DMPO) aqueous solution under different testing conditions. As observed in Fig. S12, there is no noticeable EPR signal on the curve of DLNU-M-CdS(H₂TD) MOF in the absence of light-irradiation. However, upon UV-light irradiation for 2 min, the characteristic peaks originated from the adduct of DMPO-•OH can be detected on the DLNU-M-CdS(H₂TD) MOF. It confirms that the photoinduced holes on the VB of the DLNU-M-CdS(H₂TD) MOF can oxidize H₂O molecule into •OH (the EPR peaks with the intensity ratio of 1:2:2:1). Interestingly, when adding the TEOA into the above DMPO aqueous solution, the signal intensity of the DMPO-•OH adduct for the sample of DLNU-M-CdS(H₂TD) MOF was obviously decreased under UV-light irradiation for 2 min. This observation suggests that the photoinduced holes on the VB of the DLNU-M-CdS(H₂TD) MOF can be captured preferentially by the TEOA in the aqueous solution, leading to effectively hinder the recombination of the photoinduced

electron-hole pairs. That is to say, the electron-donating process occurs from the TEOA to the DLNU-M-CdS(H₂TD) MOF during the photocatalytic H₂ evolution.

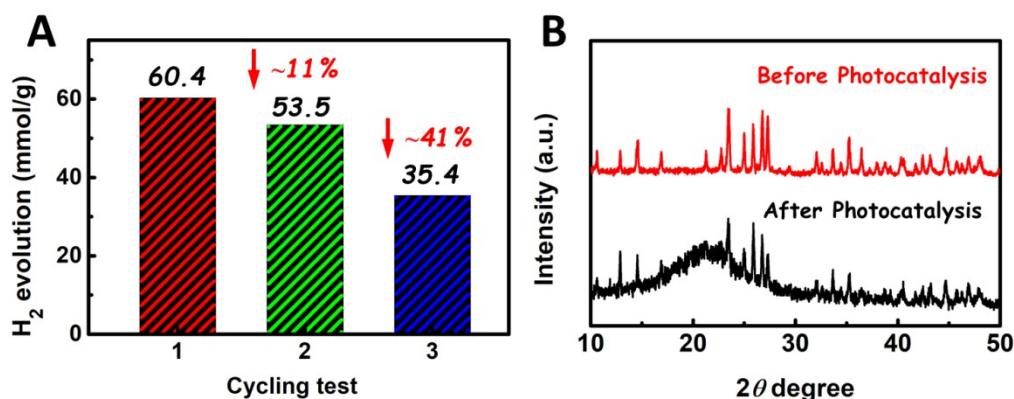


Fig. S13 (A) cycling test of photocatalytic H₂ evolution over the DLNU-M-CdS(H₂TD) MOF under UV-visible-light irradiation for every 3 hours; (B) XRD patterns of the DLNU-M-CdS(H₂TD) MOF before and after photocatalysis.

The cycling test of photocatalytic H₂ evolution over the DLNU-M-CdS(H₂TD) MOF has been carried out under UV-visible-light irradiation for every 3 hours. The result shows that the photocatalytic H₂-evolution amount of the DLNU-M-CdS(H₂TD) MOF gradually decreases during the cycling test (Fig. S13A). After the three-run test, the photocatalytic activity of the DLNU-M-CdS(H₂TD) MOF could only maintain ~59% of the initial activity as compared to the first cycle. In order to investigate the reason of this decreased photocatalytic activity, the XRD pattern of the DLNU-M-CdS(H₂TD) MOF after the photocatalysis was tested. As observed in Fig. S13B, although the main diffraction peaks of the DLNU-M-CdS(H₂TD) MOF still exist after the photocatalysis, the intensities of these peaks are weakened obviously. Meanwhile, some diffraction peaks of the DLNU-M-CdS(H₂TD) MOF disappear after the photocatalysis. These observation suggests that the DLNU-M-CdS(H₂TD) MOF is not stable enough due to the photocorrosion process, which is similar with most of the MOF photocatalysts.^[4-9]

References:

- [1]. Z. Zhang, J. Huang, Y. Fang, M. Zhang, K. Liu and B. Dong, *Adv. Mater.*, 2017, **29**, 1606688.

- [2]. Z. Zhang, X. Jiang, B. Liu, L. Guo, N. Lu, L. Wang, J. Huang, K. Liu and B. Dong, *Adv. Mater.*, 2018, **30**, 1705221.
- [3]. M. J. Berr, P. Wagner, S. Fischbach, A. Vaneski, J. Schneider, A. S. Sussha, A. L. Rogach, F. Jäckel and J. Feldmann, *Appl. Phys. Lett.*, 2012, **100**, 223903.
- [4]. J. D. Xiao and H. L. Jiang, *Acc. Chem. Res.*, 2019, **52**, 356–366.
- [5]. T. Zhang, Y. Jin, Y. Shi, M. Li, J. Li and C. Duan, *Coord. Chem. Rev.*, 2019, **380**, 201–229.
- [6]. L. Jiao, Y. Wang, H. L. Jiang and Q. Xu, *Adv. Mater.*, 2018, **30**, 1703663.
- [7]. W. Wang, X. Xu, W. Zhou and Z. Shao, *Adv. Sci.*, 2017, **4**, 1600371.
- [8]. J. Wang, Y. Liu, Y. Li, L. Xia, M. Jiang and P. Wu, *Inorg. Chem.*, 2018, **57**, 7495-7498.
- [9]. P. Wu, M. Jiang, Y. Li, Y. Liu and J. Wang, *J. Mater. Chem. A*, 2017, **5**, 7833-7838.